Amperometric Aptasensor for Amyloid-beta Oligomer Detection with Optimized Stem-loop Structures and Adjustable Detection Range

Yuting Zhang,[†,∥] Gabriela Figueroa-Miranda,[†,∥] Christian Zafiu,[‡], Dieter Willbold,[‡,§], Andreas Offenhäusser,[†,∥] Dirk Mayer*[,†]

[†]Institute of Complex Systems (ICS-8), Forschungszentrum Jülich GmbH, 52428 Jülich, Germany

[∥]Faculty I, RWTH Aachen, 52062 Aachen, Germany

[‡]Institute of Complex Systems (ICS-6), Forschungszentrum Jülich GmbH, 52428 Jülich, Germany

[§]Institut für Physikalische Biologie, Heinrich-Heine-Universität Düsseldorf, 40225 Düsseldorf, Germany

KEYWORDS Amyloid-β oligomers, Alzheimer's disease, ssDNA aptamer, Stem-loop, Atomic force microscopy

ABSTRACT: Amyloid-β oligomers (AβO) have become a representative biomarkers for early diagnosis of Alzheimer's disease. Here, we report on an aptasensor based on stem-loop probes for a sensitive and specific detection of Aβ oligomers by an amperometric transducer principle using alternating current voltammetry (ACV). Stem-loop probes with redox-active moieties are immobilized on a gold substrate as receptor element. The signal transduction mechanism relies on redox ferrocene (Fc) reporting via charge transfer on a molecular recognition event involving a conformational change of the molecular beacon. The stem-loop structures were optimized by considering the aptamers' stem length, spacer, and different ferrocene terminals. In addition, the sensor assembly and signal recording including aptamer concentration and ACV frequency dependence are discussed. Using the optimized stem-loop probe (B-3' Fc), the aptasensor showed a decrease of the Fc peak current induced by AβO binding within the broad concentration range spanning six orders of magnitude. Furthermore, the detection limit of the sensor can be further decreased by optimizing the ACV frequency, however at the costs of a narrowed detection range. In this work a label-free electrochemical aptasensor is demonstrated that facilitates the quantification of the concentration of Aβ oligomers with high selectivity and subpicomolar sensitivity, which may be conducive to improve the diagnosis and pharmacology studies of Alzheimer's disease.

Alzheimer's disease (AD) is the most common chronic neurodegenerative disease characterized by progressive and irreversible cognitive decline.[1] Fibrous amyloid plaques in human brain slices have implicated that the pathological causes of AD are closely related to amyloid β (Aβ) peptide aggregation. In the past long time, insoluble Aβ fibrillary aggregates found in extracellular plaques have been thought to be the main reason of AD.[2] Recent experimental studies on Aβ peptide as well as various animal model studies suggest that small, aqueously soluble oligomeric forms of amyloid-β are more cytotoxic than fibrillar Aβ aggregates. Those first ones also inhibit many critical neuronal activities, including long-term potentiation (LTP), alter synapse physiology and memory loss in vivo and in culture soluble forms of Aβ assemblies cause substantial neuronal dysfunction even before the appearance of amyloid plaques.[3,4] Therefore, soluble amyloid-β oligomers (AβO) have been used as believable molecular biomarkers for AD early diagnosis and therapy targets for clinically therapeutic intervention.

Many methods have successfully implemented the detection of AβO, for example, sFIDA, SPR biosensor, fluorescent sensor, and ELISA.[5-8] These methods are usually time-consuming, high operation cost, labor intensive or lack selectivity. Therefore, there is a continuing demand for simple and sensitive methods for the selective assay of neurotoxic AβO. Electrochemical biosensors represent a rapid, cost-effective, highly sensitive alternative for analyte detection at the point-of-care. Electrochemical biosensors are widely used for monitoring biomarkers of patients with chronical diseases and possess great miniaturized and personalized potential for medicine (diagnostic tests to guide therapy) due to the fast response, high sensitivity, and simple operation.[9] However, there is still a great challenge for AβO assay due to the coexistence of Aβ monomers and fibrils in samples. Moreover, ultralow concentration detection of AβO is required, which call for a low limit of detection (LOD) to support accurate diagnosis and reduce the amount of sample.

To address this issue, aptamers with high affinity and specificity for AβO were selected by the combination of a gel-shift assay and a competitive screening method.[10] Aptamers are single-stranded DNA or RNA sequences isolated from nucleic acid libraries via Systematic Evolution of Ligands by Exponential enrichment (SELEX).[11] They are known to interact with its respective targets by form conformational unique 3-dimensional structures.[12] Molecular beacons (MB), first developed by Tyagi and Kramer in 1996, are single stranded oligonucleotide probes that adopt a stem-loop configuration by intramolecular base pairing with a fluorophore/quencher pair that possess a stem-loop structure. MB are mainly used for DNA sequence detection based on changes in fluorescence intensity.[13] In addition to optical biosensors, MB can also be replaced their fluorophores with redox groups for electrochemical probes.[14] The stem-loop structured DNA probes are superior to linear probes in several aspects for the detection of target molecules.[15] The greatest advantage regarding stem-loop aptamers is the strong conformational change induced by the target binding and the reduction of the degree of freedom of the aptamer, which leads to increased background currents due to unspecific charge transfer.

In our previous work, an impedimetric label-free aptasensor utilizing an AβO specific aptamer has been proposed and used to monitor the Aβ peptide aggregation, however the limit of detection is still in the range of several tens of picomol due to the impedimetric transducer principle.[16] To further improve the sensitivity of the aptasensor towards AβO, we report in this work on a novel molecular beacon-based electrochemical aptamer-based (E-AB) sensor for amperometric detection of AβO. To our knowledge, this is first work related to immobilization process and stem-loop structures optimization of aptamer specific to AβO. Amperometric detection schemes rely on charge transfer between the electrode and redox probes that are either attached to the receptor and/or diffuse in the solution phase.[17,18] Here, alternating current voltammetry (ACV) was used to operate the sensor with surface confined redox processes, which facilitates low noise levels and in principle also simultaneous detection of various targets. The surface tethered stem-loop probes are dually labeled with a thiol group at the proximal end for surface coupling and a redox group ferrocene (Fc) at the distal end for signal reporting. To optimize the aptasensor sensitivity for AβO, variations of the stem-loop aptamers' structures including stem number, ssDNA length, location of redox probe at 3' or 5' terminal end, and spacer length are tested. Furthermore, aptamer immobilization concentration and the ACV detection parameters are studied. The obtained amperometric aptasensor was found to exhibit not only a high sensitivity, selectivity and reproducibility for AβO detection but also an adaptable range of detection and detection limits down to the sub picomolar range by appropriate selection of ACV signal recording conditions. Our aptasensor provides reliable and reproducible data for the quantification of a target molecule, which can endow affordable biosensors with superior sensitivity and specificity.

EXPERIMENTAL SECTION

Chemicals and devices. DNA oligonucleotides used in this work were HPLC-purified and obtained from FRIZ Biochem Gesellschaft für Bioanalytik GmbH (Neuried, Germany). The sequences are listed in Table S1 and their structures are shown in Scheme 1. Tris (hydroxy-methyl)-aminomethane hydrochloride (Tris-HCl), sulfuric acid, magnesium chloride, sodium chloride, tris-(2-carboxyethyl) phosphine hydrochloride (TCEP), potassium chloride, 1,1,1,3,3,3-hexafluoro-2-propanol (HFIP), and 6-mercapto-1-hexanol (MCH) were purchased from Sigma-Aldrich. Ethanol and isopropanol were obtained from Merck. Aβ peptide (Aβ1-40, 4 kDa) was purchased from Peptide Institute Inc. (Japan). All other chemicals were analytical grade.

All of the solutions were prepared with Milli-Q water purified through a Milli-Q ultrapure water system (18.25 MΩ cm, Gradient A10, Merck Millipore, Burlington, USA). The following buffers were used in this study: high salt Tris-HCl buffer (10mM Tris, 1.5 M NaCl, 1 mM $MgCl_2$, pH 7.4), low salt Tris-HCl buffer (10mM Tris, 150 mM NaCl, 5 mM KCl, pH 7.4). Artificial cerebrospinal fluid (aCSF) was prepared by dissolving 150 mM NaCl, 3.0 mM KCl, 1.4 mM $CaCl_2{\cdot}2H_2O$, 1 mM NaH_2PO_4, and 0.8 mM $MgCl_2{\cdot}6H_2O$ in MilliQ water. In order to demonstrate the potential usefulness of the developed sensor, 45 mg dL^{-1} human serum albumin was added to the aCSF to imitate detection conditions as realistic as possible. Aβ peptides including Aβ monomers (AβM), AβO, and Aβ fibrils (AβF) were prepared as described by Tsukakoshi et al (see Supporting Information).[10]

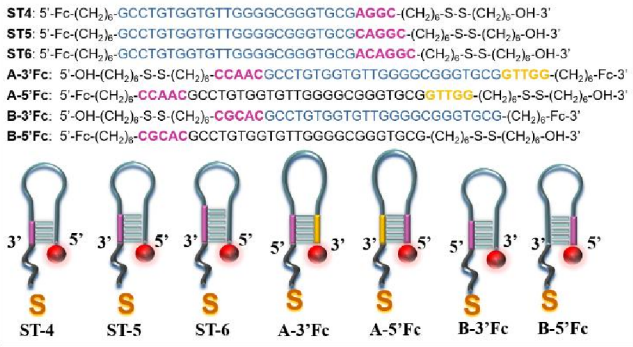

Scheme 1 Mechanism for aptasensor detection based on a stem-loop aptamer.

Electrode cleaning and pretreatment. Prior to surface coating, the gold rod working electrode (AuR) was polished sequentially using alumina slurries with the diameter 0.3 μm and 0.05 μm for 5 min to become specular. Then, the polished AuR was ultrasonically cleaned in ethanol, isopropanol and Milli-Q water for 5 min, respectively. The rinsed electrode was electrochemically cleaned in 0.5 M NaOH (voltage sweeps from –1.5 V to 0 V, 500 scans at a scan rate of 4 V s^{-1}) and 0.5 M H_2SO_4 (voltage sweeps from 0 V to 1.5 V, 100 scans at a scan rate of 1 V s^{-1}) by cyclic voltammetry to obtain a clean gold electrode

surface. The Electrode area can be determined by running a cyclic voltammetry (CV) cycle in a fresh 0.05 M H_2SO_4 solution from 0 V to 1.35 V at a scan rate of 0.1 V s^{-1}.[19] Finally, the electrode was rinsed with Milli-Q water and dried at ambient temperature for further use.

Preparation of the aptasensor. The DNA stock solution was activated in 10 mM TCEP for 1 h to cleave disulfide bonds and then diluted to different concentrations with high salt concentration Tris-HCl buffer. Self-assembly was carried out by inserting the cleaned gold electrodes in 400 µL thiolated stem-loop ssDNA solution in the dark for overnight. After that, the electrode was slowly rinsed with 3 mL Milli-Q and Tris-HCL buffer to remove non-bonding materials. The above electrode was immersed in 0.1 mM MCH for 1h to prepare a compact self-assembled monolayer (SAM) by covering the remaining bare regions. Finally, to remove the unattached MCH and any excess probe DNA physically adsorbed on the electrode surface, the electrode was rinsed thoroughly to obtain the stem-loop aptasensor with 6 mL Tris-HCl buffer and Milli-Q water. For AβO assay, the aptasensor was incubated in various concentrations of the complementary target for 30 min. After incubation, the electrode was rinsed by Tris-HCl buffer to remove non-specifically adsorbed target AβO.

Electrochemical measurements. All measurements were performed on a three-electrode cell at room temperature, including the gold rod electrode with 2 mm diameter (AuR) as working electrode, a platinum wire as counter electrode, and a saturated Ag/AgCl electrode as reference electrode. ACV measurements were performed using an Autolab PGSTAT302 (Eco Chemie, Netherlands) with NOVA software in Tris-HCl buffer (10 mM Tris, 150 mM NaCl, 5 mM KCl, pH 7.4). ACV scans ran between 0 V and 0.6 V with potential steps of 0.005 V, modulation amplitude 0.025 V, modulation time 0.4 s and interval time 0.8 s. All experiments were carried out at least three times to ensure the repeatability of the response trend and calculate the relative standard deviation (R.S.D). The concentrations of aptamers and AβO were determined with a UV/Vis/NIR spectrometer Lambda 900 (Perkin Elmer, USA).

AFM measurements. AFM imaging was performed using a Nanoscope Multimode 8 microscope (Bruker) equipped with a piezoelectric scanner and aluminum back coated Si cantilevers from Bruker (OTESPA-R3) with a resonant frequency range of AFM cantilever 115 – 300 Hz, and number of pixels 512 × 512 at scan rate 1 Hz, scan size 0.5 µm. A bare gold (111) single crystal disk was used as model electrode surface. The activation and cleaning of the single crystal was done by thoroughly rinsing it in ethanol, isopropanol, and Milli-Q water. After drying, the crystal were annealed for 10 min in a hydrogen flame and cooled down to room temperature in an argon stream. The subsequent aptamer modification and target detection were done as described in section 2.4.

RESULTS AND DISCUSSION

Principle of the aptasensor. To construct an amperometric Fc-based aptamer biosensor for AβO, we employed surface-immobilized stem-loop ssDNA molecules as recognition elements and ferrocene as redox label. The stem-loop receptor, dually labeled with thiol and ferrocene, has been designed such that it has two five-base sequences at the terminal ends of the aptamer-probe, so that the DNA strand will be closed and form a double-stranded stem structure by thermostable paring. The concept of AβO detection based on a stem-loop aptamer is shown in

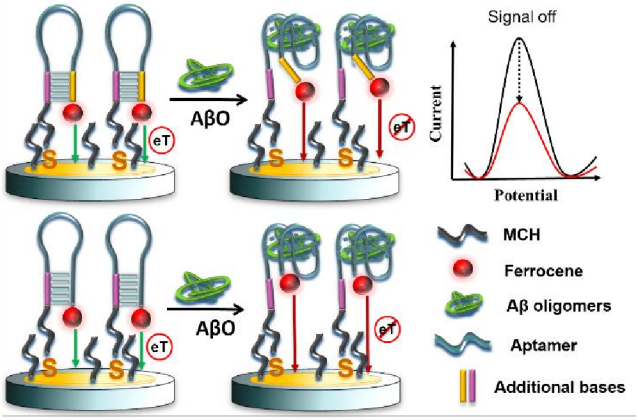

Scheme 2 Oligonucleotide sequences used in this work. Red letters indicate nucleotides that were inserted into the original aptamer sequence to form a stem loop either with nucleotides of the original aptamer sequence ((blue letters) or with inserted nucleotides (pink / yellow letters) at the end of the DNA.

Scheme 2. After cleaning the gold electrode surface, the stem-loop probe is assembled at the electrode interface to form a SAMs through DNA-thiol bonding. Then the remaining uncovered areas of the electrode are blocked by MCH decreasing unspecific adsorption. Directly after the formation of the mixed monolayer, the immobilized stem-loop probes exist in their "closed" state in the absence of target AβO, at which the ferrocenes are localized close to the electrode surface facilitating an efficient electron transfer and consequently enabling the measurement of high redox currents. After administration of the target AβO, it binds to the ssDNA and brakes the stem, which causes a transformation of the DNA into the "open" conformation. This increases the distance between ferrocene and the electrode surface, which diminishes the charge transfer current. Since the electron transfer depends exponentially on the distance between donor and acceptor, even small changes in the aptamer conformation can be efficiently probed by the amperometric detection scheme.

Atomic force microscopy (AFM) was used to investigate the step by step modification of the sensor electrode and the binding of AβO to the aptamer modified surface (Figure 1). A bare gold (111) single crystal disk was analyzed by AFM as a reference surface to provide a surface smooth enough to allow an unambiguous mapping of morphological changes during surface modification. Figure 1 shows three rows of images with the top view topography in the first row, a cross section corresponding to the respective

white lines in the second row, and a 3D image in the bottom row to visualize the stepwise increase of the surface roughness.

The AFM images of the bare Au electrode exhibit atomically flat Au terraces with monoatomic steps (step height approx. 2Å) on the left side (Figure 1A, E, and I).[20] The corresponding cross-section shows a flat line with sub-Å corrugations originating mainly from the noise of the AFM system indicating a clean and adsorbate free surface. After aptamer immobilization, several 3D topographical features can be observed. Firstly, one can still see monoatomic steps and also holes. The latter can be assigned to defects in the topmost gold layer generated during aptamer immobilization, which is commonly found for thiol-based SAMs.[21,22] Secondly, corrugations are present on the terrace as well as surrounding the monoatomic holes, which possess feature heights of around 1 nm and can presumably be assigned to unordered aptamer molecules, (Figure 1B, F, and J). Since the concentration of the aptamer solution was low and no blocking MCH was applied until this preparation step, it can be assumed that the immobilized ssDNA lie down on the surface, which is supported by the small feature height (smaller than aptamer length). After blocking the remaining free Au areas with MCH, the monoatomic defects disappeared. The surface exhibits a large number of homogeneously distributed hillocks (Figure 1C and G) with heights of 1.5 nm ± 0.5 nm (see particle analysis, Supporting Information, Table S2), suggesting that the aptamer receptors form small domains of generally upstanding ssDNA surrounded by short chain MCH molecules. Apparently, a phase separation takes place between polyanionic aptamers and MCH with hydrophobic alkyl chains. At last, the surface morphology of the Au crystal was studied after its incubation in AβO medium. The AFM analysis revealed a significant increase in the height of the hillocks confirming the formation of aptamer/AβO complexes with heights of 3.1 nm ± 0.9 nm. The surface roughness of the Au crystal continuously increased during the modification sequence from bare gold, via aptamer and MCH adsorption to the AβO binding from 0.08 nm, 0.33 nm, 0.51 nm to 0.94 nm, respectively. These results are also manifested in the corresponding 3D AFM height images (Figure 1I-L) and particle analysis (see Supporting Information, Figure S1 and Table S2).

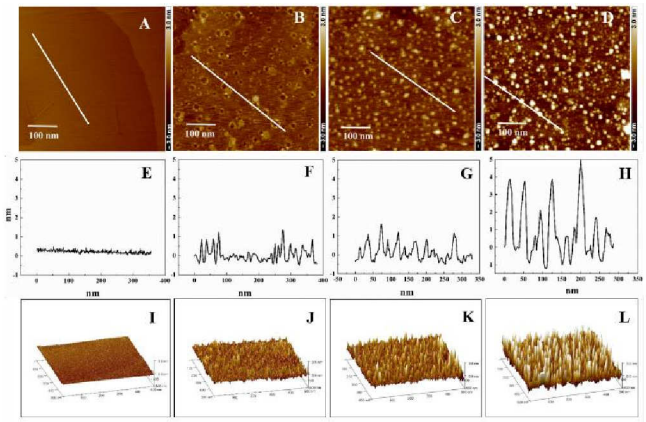

Figure 1 Tapping mode AFM images of gold surface before (A) and after aptamer (B), MCH (C), and AβO (D) surface immobilization. Cross-section analysis (E–H) and 3D AFM height images (I–L) corresponding to A–D, respectively.

Comparison of the aptamer Stem-Loop structures. The aptamer oligonucleotide used in this work was selected by Tsukakoshi *et al.*[10] using a competitive screening method.[17] In our work, we intended to develop an aptasensor containing a stem-loop that shows signal off characteristics, means that the redox current drops after target binding. In order to find the optimal stem-loop configuration with the highest signal response, the stem length, spacer length, and position of the ferrocene terminus were altered. The relative suppression (SS) of the ferrocene faraday current $(I–I_0)/I_0$ (%) was determined as the sensor signal.

Effect of the Stem Length. The stem length is a key parameter that determines the response of the ssDNA-Fc strand to its target. If the stem is too long or short, the hairpin-like conformation doesn't open or opens too easily, affecting the response signal of ferrocene upon target administration. Hence the stem length of the stem-loop must be properly chosen in order to obtain an optimal balance: strong enough to form the hairpin structure but also weak enough to be dissociated when target AβO binds to the aptamer. Each base pair contributes to the stem loop by a binding energy ΔG of approximately 5 kJ/mol.[23] The binding energy to the target needs to exceed the energy sum of all base pairs. To obtain the optimal stem length, we designed three DNA stem-loop probes that contain different stem lengths between 4 and 6 base pairs (ST-4, ST-5, and ST-6, shown in Table S1 and Scheme 2) and tested the sensing performance of the corresponding aptasensors. Their responses to the same concentration of AβO targets (10 pM) are shown in Figure 2A–C. Electrodes modified with ST 4 show unstable and random ACV peak currents. The black lines represent responses of the aptasensor in Tris-HCl buffer without AβO (blank). The current response was unstable and increased with the number of scans, indicating transient stem-loop formation. After adding 10 pM AβO, the current decreased a little but subsequently increased again (red lines). These results demonstrate that a stem length

of 4 base pairs is too short for our ssDNA sequences to form a sturdy and stable stem-loop structure. For the blank ST-5 probe, the current response became reproducible for repeated ACV scans. After adding 10 pM AβO, the ST-5 aptasensor showed (34.8 ± 2.0) % SS, while the aptasensor containing ST-6 exhibited only (20 ± 3.6) % SS. The signal difference between ST-5 and ST-6 suggests that the stem formation strongly competes with the target binding, if six stem base pairs are used. Consequently, the stem structure is conserved, even if the target is present for many of the surface tethered aptamer receptors and the distance between Fc and electrode surface does not change sufficiently. Among different aptamers with different stem length, the ST-5 showed the best detection performance towards AβO. Therefore, we chose the ssDNA sequence containing a stem-loop with 5 base pairs (ST-5) for the subsequent tests.

In the following, two additional design motifs are introduced for our oligonucleotide aptamers namely additional based pairs that are forming the stem and the location of the redox probe as well as the thiol linker, are inverted. At first, additional stem forming bases were added either on both sides of the aptamer strand or alternatively, on only one end leading to ssDNA molecules with 34 (named Probe A) and 29 bases (named Probe B), respectively. Probe B forms the stem between additional and own bases while Probe A uses exclusively additional bases for the stem on both terminal ends. The second design motif concerns the location of the thiol linker and the redox probe. DNA with thiol at the 5' end and ferrocene at the 3' end are named 3' Fc. Conversely the DNA with 3' end thiol and 5' end ferrocene are termed as 5' Fc.

Effect of the oligonucleotide length. Comparing the SS of the different aptamer receptors responding to 10 pM AβO, aptamer A always gave a lower signal decrease than aptamer B, independent whether the redox probe was located at the 3' or 5' terminal end, Figure 2D. This might be caused by two main reasons: firstly, aptamer B is shorter than aptamer A, tending to form more compact and stable SAMs. Singh *et al.* reported that single-stranded DNA with short chains (less than 10 bases) or long chains (more than 30 bases) does not produce appropriate films because of the self-protection mechanism observed during DNA surface film formation.[24] This means that long chains will intertwine with neighboring strands rather than interacting with the electrode material, inhibiting the film growth. Second: the long sequence of aptamer A makes the formation of stem-loop structures less favorable due to entropic reasons.[25] Therefore, short-length aptamer B oligonucleotides including 29 bases were chosen for the further design optimization of the stem-loop DNA probe for AβO sensing.

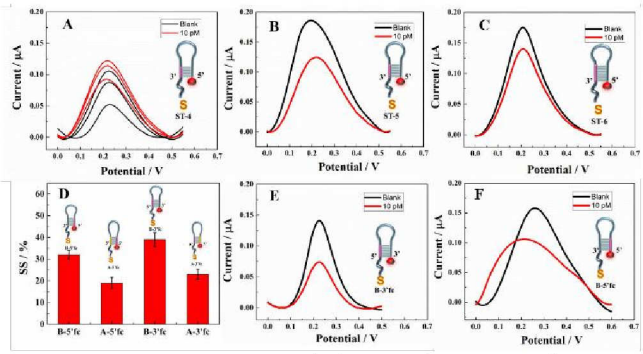

Figure 2 ACV curves recorded towards 10 pM AβO in 10 mM Tris-HCl + 150 mM NaCl + 5 mM KCl at ST-4 (A), ST-5 (B), and ST-6 (C) aptasensor; (D) The SS of the different oligonucleotide-length aptamer sensors A-3'Fc, A-5'Fc, B-3'Fc, and B-5'Fc responding to 10 pM AβO; The effect of location of thiol and ferrocene (B and E) and spacer (B and F) on AβO response.

Location of thiol and ferrocene at 3' or 5'. The position of the thiol binding and Fc redox group also affects the aptamer sensing performance for the same DNA oligonucleotide sequence and length. A comparison of current response of ST-5 (5' Fc, Figure 2B), B-3'Fc modified electrodes (Figure 2E) exhibited a higher SS of 39 ± 1.2 % in comparison to 34.8 ± 2.0 %, respectively, which can be attributed to two differences in the stem-loop structure. On the one hand, narrow and well defined peaks are obtained for 3'-terminal Fc aptamers, while aptamers with redox probes attached to the 5'-terminal end showed broad peak shapes. This is because the 3' Fc group reaches the electrode surface easily and facilitate a reversible heterogeneous electron transfer.[26] The total amount of 3' terminal Fc group can be correlated quantitatively to the height of the anodic or the cathodic peak corrected from the background current.

On the other hand, also the attachment of the two aptamer receptors on the electrode is different due to the opposite position of the thiol binding moiety. 3' thiol groups can access to gold surface better than those attached to the 5'-terminal end, enables higher surface density of aptamer receptors.[27] The estimation of the aptamer density by chronocoulometry confirms this assumption (see Supporting Information, Figure S2). The density of B-3'Fc aptamers deposited from 1.0 µM solutions is with 2.75 $*10^{12}$ molecules cm^{-2} nearly 50 % smaller than those of B-5' Fc aptamers deposited from a solution of the same concentration. This low value for B-3'Fc aptamers indicates that the chains are sparsely grafted on the electrode surface as non-interpenetrating polymer coils.[28] Our aptamers form a parallel G-quadruplex structures after target binding, which is relatively bulky and requires much space for AβO recognition. It should be noted that optimal stem-loop ssDNA probe density is 2.4 – 5.0 times lower than that of linear ssDNA probes on the same surfaces,[29] indicating that the stem-loop requires more space to unfold upon target immobilization. Hence, 3'-terminal redox and 5'-terminal thiol labeling provides apparently the highest SS and is therefore the most ap-

propriate single-stranded oligonucleotide receptor for the detection of AβO.

Effect of spacer. Another possible aspect that contributes to the large SS (39 ± 1.2 %) of B-3' Fc in comparison to B-5' Fc (31.9 ± 1.9 %) modified receptors is that the added bases are located at the terminal bound to the surface, which could act as a spacer for B-3' Fc. In order to study the effect of a spacer group on the sensor performance, we compared the response of AuR electrodes modified with B-5' Fc and ST-5 modified (Fc also on 5' terminal end) towards administration of 10 pM AβO. Figure2B and F show that ST-5 modified AuRs exhibit a bigger signal decrease of about 34.8 ± 2.0 % than that of B-5' Fc of 31.9 ± 1.9 %. Moreover, the ST-5 modified sensors (Figure 2B) exhibited a stable peak potential before and after AβO binding compared to B-5' Fc modified sensors (Figure 2F). It has been reported that aptamers, where the unit undergoing the conformational change is located close to the electrode surface, may not be able to fold into the three-dimensional structure necessary for target recognition due to steric hindrance.[30] Therefore, the incorporation of a spacer can render a molecular probe attached to a solid support more accessible to its target, which has been proven to be an effective strategy to increase the sensitivities of ssDNA based sensors.[31] In summary, considering the effects of stem length, oligonucleotide length, thiol and Fc terminal position, and spacer, oligonucleotide B-3'Fc exhibits the highest signal and is chosen as the optimal receptor in the next experiments.

Optimizations of the analytical parameters. Since the breaking of the stem affects the dynamics of the DNA associated redox probe signaling, the sensor performance sensitively depends on the receptor immobilization condition, which can affect the blank (background) and the target responses, see above. To determine the optimal receptor concentration, Fc tagged aptamer probes were immobilized on the AuR electrodes in a concentration range of 0.1 to 1.5 µM (see Supporting Information, Figure S3). A concentration of 1.0 µM aptamer was found to give the highest value of $\Delta I/I_o$. This concentration of Fc tagged ssDNA receptors was used for all subsequent experiments.

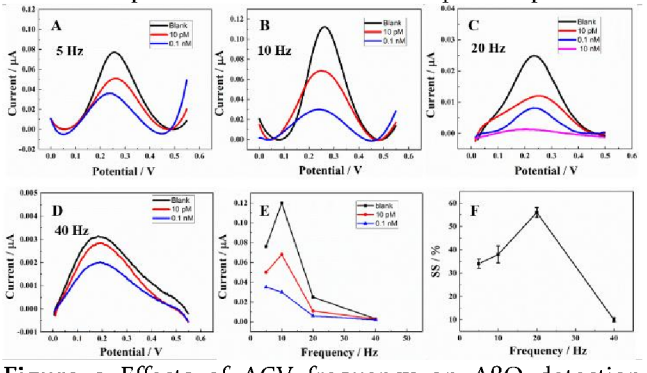

Figure 3 Effects of ACV frequency on AβO detection response from 5 to 40 Hz: A–D: ACV responses of aptasensor towards different concentrations of AβO; E: aptasenor responses to blank, 10 pM, and 0.1 nM AβO at different frequency; F: aptasenor responses towards 10 pM AβO at different frequency.

Further, to elucidate the influence of the incubation time on AβO binding, the aptasensor response after 10 min to 50 min analyte exposure were recorded and shown in Fig. S3B. A saturation of the sensor signal was achieved after 30min. Considering sensor response and efficiency, an incubation time of 30 min was used for all further experiments.

Next, the effect of the applied AC frequency on the signal gain was investigated. For amperometric sensors that employ a surface-immobilized reversible redox label, the redox signal depends inherently on the applied frequency in ACV measurements (Figure 3).[32] For B-3' Fc receptors (Figure 3E), the redox current from Fc group increased between 1 Hz and 10 Hz and dropped from 10 Hz to 40 Hz in the absence of AβO (blank). A similar trend was observed for sensors in the target-bound state (10 pM and 0.1 nM AβO). The peak current should be proportional to the AC frequency when the frequency is sufficiently lower than the electron-transfer rate. However, as the applied frequency reached a threshold value where electron transfer can no longer keep up with the oscillating potential, the peak current diminished relative to the background current.[33] Since the % SS is determined using both the pre- and post-binding currents, it also depends on the applied frequency. The distance between redox group and electrode is larger for the target bound state of the aptamer in comparison to the stem-loop, which results in a drop of the current at lower frequencies for the former. The relative difference between target bound and stem-loop currents was largest for 20 Hz, which can be considered as the optimal AC frequency providing the best sensitivity of the target detection. However, the high sensitivity came on the costs of a smaller detection range, since the currents droped to zero already at relatively low analyte concentrations of 10 nM AβO or higher. Therefore, we chose 20 Hz for the detection of low amounts of AβO, and 10 Hz to achieve a wide dynamic range of detection.

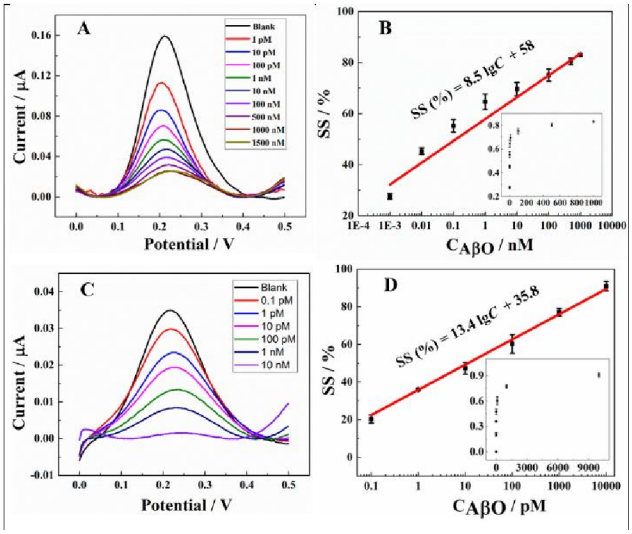

Figure 4 (A) ACV curves obtained at B-3' Fc modified AuR upon different concentrations of AβO applied 10 Hz, (B) The calibration curve for AβO from 1 pM to 1500 nM.

(C) ACV curves obtained at B-3' Fc modified AuR upon different concentrations of AβO from applied 20 Hz, (D) The calibration curve for AβO from 0.1 pM to 10 nM.

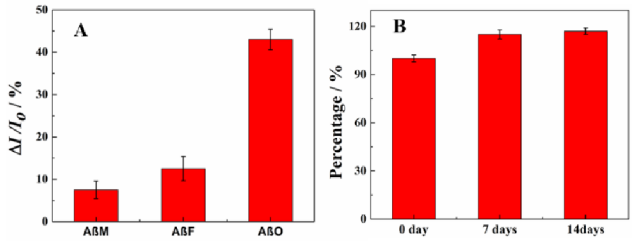

Figure 5 (A) Selectivity of the developed aptasensor towards 10 pM AβM, AβO and AβF in 10 mM Tris-HCl + 150 mM NaCl + 5 mM KCl. (B) Stability of the aptasensor signal towards 1 pM AβO stored in 4°C fridge for 7 days and 14 days.

Performance of aptasensor for AβO. To demonstrate the versatility of the optimized oligonucleotide probe, we used AuR electrodes modified with B-3' Fc oligonucleotide probe to detect AβO via disrupting the stem-loop structure. The sensitivity of the electrochemical aptasensor for the target assay was determined by varying the AβO concentrations. The sensor showed a logarithmic concentration-dependence in the range from 1.0 pM to 1500 nM, saturating at 1500 nM, when a frequency of 10 Hz was applied (Figure 4A). The calibration equation was SS (%) = 8.5 lg*C* + 58 with a correlation coefficient of 0.991 (Figure 4B). The signal at detection limit was $6.5*10^{-6}$ nM defined as 3 times the standard deviation and the blank signal. Similarly, at an applied frequency of 20 Hz, the SS possessed a logarithmic dependence on the AβO concentration from 0.1 pM to 10 nM. The calibration curve was determined to be SS (%) = 13.4 lg*C* + 35.8 with a correlation coefficients of 0.999 (Figure 4C and D). At an applied frequency of 20 Hz, the aptasensors possessed a narrower linear range (from 0.1 pM to 10 pM) but a lower detection limit of 0.002 pM compared to the situation where a frequency of 10 Hz is applied. Compared to the existing AβO assays (Table S3, the Supporting Information), the proposed aptasensor showed lower detection limits and has a wider concentration detection range. The sensor is sensitive enough for the detection of low concentration of AβO in aCSF and covers the human physiological levels for AβO. More importantly, this method obviates the utilization of enzyme-linked antibody and expensive instruments, thus reducing the operational complexity and assay cost.

To evaluate the selectivity of the ssDNA molecular beacon against AβO, control experiments were performed using 10 pM AβM and AβF as interfering targets. As shown in Figure 5A, a significant SS of about 40% was observed induced by the interaction of the aptamer probe with AβO, while the signal caused by the other Aβ peptides was significantly lower. Nevertheless, there was also an approximately 10% SS caused by the presence of AβM and AβF for our aptasensor, maybe owing to residual AβO generated during the preparation of AβM and AβF samples. However, this result indicates that AβO binds to its aptamer with higher affinity than other Aβ forms and the molecular oligonucleotide redox beacon shows a high selectivity toward AβO.

The long-term stability and reproducibility of the sensing interface are important factors for the development and practical implementation of an aptasensor. The stability of the electrochemical aptasensor was tested over a period of two weeks, Figure 5B. After each measurement, the aptamer sensor was stored in a Tris-HCl buffer solution at 4 °C. It was observed that the aptasensor could still retain within 80% of its initial response, indicating that the developed aptasensors attain a sufficient stability for AβO detection. The relative standard deviation (R.S.D.) of reproducibility at one modified electrode was calculated to be 1.2% for 3 successive determinations of 10 pM AβO. For 3 different aptasensors, the R.S.D was 3.0%.

AβO levels in cerebrospinal fluid is related to AD pathology, therefore the detection assay of AβO in real samples could become a powerful tool for clinical diagnosis of AD. To demonstrate the versatility of this aptasensor, AβO detection was tested in aCSF containing human serum albumin, as illustrated in Table S4. Our data showed acceptable conformance of 108% to 119% with data obtained for the calibration curves, indicating good accuracy and validity of the developed assay for AβO detection in aCSF samples with proteins.

CONCLUSION

In this work, a simple and sensitive aptasensor based on ssDNA stem-loop probes is proposed for the selective detection of AβO by amperometric response change using ACV. To obtain satisfactory performance, we have optimized systematically the stem-loop structures, including stem number, oligonucleotide length, location of redox probes, sequence, and spacer. At the end, a stem loop with 5 base pairs and a ferrocene label attached to the 3' terminal end was found to possess the highest signal change caused by target binding. The proposed aptasensor exhibited a wide concentration detection range from 0.1 pM to 1500 nM with a low detection limit at a fM level, which is sensitive enough for the detection of physiological concentration of AβO. We also found that the detection range can be adjusted by varying the ACV frequency, which facilitated either a low detection limit or a broad detection range. A long-time stability test yielded 80% conservation of the original signal after a two-week storing period. In addition, a considerable selectivity towards AβO over other Aβ protein species was observed. These excellent sensor features as well as its other characteristics, such as easy fabrication and operation convenience, make our new aptasensor a promising alternative to conventional AβO analysis methods for early diagnosis of AD.

ASSOCIATED CONTENT

Supporting Information

The Supporting Information is available free of charge on the ACS Publications website.

Oligonucleotide sequences (Table S1); Particle analysis of AFM (Figure S1 and Table S2); Surface aptamer density ((Figure S2); Effects of concentration of aptamer on AβO response (Figure S3); Performance comparison of the proposed label-free aptasensor with other AβO sensors (Table S3); Detection of AβO in artificial CSF (Table S4) in PDF file.

AUTHOR INFORMATION

Corresponding Author

* E-mail: dirk.mayer@fz-juelich.de (Dirk Mayer), Institute of Complex Systems (ICS-8), Forschungszentrum Jülich GmbH, 52428 Jülich, Germany.

Notes

The authors declare no competing financial interest.

ACKNOWLEDGMENT

Yuting Zhang gratefully acknowledges financial support from the China Scholarship Council (No.201506890024).

REFERENCES

(1) Hardy, J. A.; Higgins, G. A. Alzheimer's disease: the amyloid cascade hypothesis. *Science* **1992**, *256*, 184.

(2) Blennow, K.; de Leon, M. J.; Zetterberg, H. Alzheimer's disease. *The Lancet* **2006**, *368*, 387-403.

(3) Glabe, C. G. Structural classification of toxic amyloid oligomers. *J. Biol. Chem.* **2008**, *283*, 29639-29643.

(4) John, T.; Gladytz, A.; Kubeil, C.; Martin, L. L.; Risselada, H. J.; Abel, B. Impact of nanoparticles on amyloid peptide and protein aggregation: a review with a focus on gold nanoparticles. *Nanoscale* **2018**, *10*, 20894-20913.

(5) Hülsemann, M.; Zafiu, C.; Kühbach, K.; Lühmann, N.; Herrmann, Y.; Peters, L.; Linnartz, C.; Willbold, J.; Kravchenko, K.; Kulawik, A. Detection of a biomarker for Alzheimer's disease from synthetic and clinical samples using a nanoscale optical biosensor. *J. Alzheimers Dis.* **2016**, *54*, 79-88.

(6) Haes, A. J.; Chang, L.; Klein, W. L.; Van Duyne, R. P. Detection of a biomarker for Alzheimer's disease from synthetic and clinical samples using a nanoscale optical biosensor. *J. Am. Chem. Soc.* **2005**, *127*, 2264-2271.

(7) Zhu, L.; Zhang, J.; Wang, F.; Wang, Y.; Lu, L.; Feng, C.; Xu, Z.; Zhang, W. Selective amyloid β oligomer assay based on abasic site-containing molecular beacon and enzyme-free amplification. *Biosens. Bioelectron.* **2016**, *78*, 206-212.

(8) Park, M. C.; Kim, M.; Lim, G. T.; Kang, S. M.; An, S. S. A.; Kim, T. S.; Kang, J. Y. Magnetic bead droplet immunoassay of oligomer amyloid β for the diagnosis of Alzheimer′ s disease using micro-pillars to enhance the stability of the oil – water interface. *Lab Chip* **2016**, *16*, 2245-2253.

(9) Lubin, A. A.; Vander Stoep Hunt, B.; White, R. J.; Plaxco, K. W. Effects of probe length, probe geometry, and redox-tag placement on the performance of the electrochemical E-DNA sensor. *Anal. Chem.* **2009**, *81*, 2150-2158.

(10) Tsukakoshi, K.; Abe, K.; Sode, K.; Ikebukuro, K. Selection of DNA aptamers that recognize α-synuclein oligomers using a competitive screening method. *Anal. Chem.* **2012**, *84*, 5542-5547.

(11) Tzouvadaki, I.; Aliakbarinodehi, N.; De Micheli, G.; Carrara, S. The memristive effect as a novelty in drug monitoring. *Nanoscale* **2017**, *9*, 9676-9684.

(12) McConnell, E. M.; Holahan, M. R.; DeRosa, M. C. Aptamers as promising molecular recognition elements for diagnostics and therapeutics in the central nervous system. *Nucleic Acid Ther.* **2014**, *24*, 388-404.

(13) Tyagi, S.; Bratu, D. P.; Kramer, F. R. Multicolor molecular beacons for allele discrimination. *Nat. Biotechnol.* **1998**, *16*, 49.

(14) Li, D.; Song, S.; Fan, C. Target-responsive structural switching for nucleic acid-based sensors. *Nucleic Acid Ther.* **2010**, *43*, 631-641.

(15) Summerer, D.; Marx, A. A Molecular Beacon for Quantitative Monitoring of the DNA Polymerase Reaction in Real - Time. *Angew. Chem. Int. Edit.* **2002**, *41*, 3620-3622.

(16) Zhang, Y.; Figueroa-Miranda, G.; Lyu, Z.; Zafiu, C.; Willbold, D.; Offenhäusser, A.; Mayer, D. Monitoring amyloid-β proteins aggregation based on label-free aptasensor. *Sensor Actuat. B Chem.* **2019**, 288, 35-542.

(17) Feng, L.; Lyu, Z.; Offenhäusser, A.; Mayer, D. Multi - Level Logic Gate Operation Based on Amplified Aptasensor Performance. *Angew. Chem. Int. Edit.* **2015**, *54*, 7693-7697.

(18) Feng, L.; Sivanesan, A.; Lyu, Z.; Offenhäusser, A.; Mayer, D. Electrochemical current rectification–a novel signal amplification strategy for highly sensitive and selective aptamer-based biosensor. *Biosens. Bioelectron.* **2015**, *66*, 62-68.

(19) Schröper, F.; Brüggemann, D.; Mourzina, Y.; Wolfrum, B.; Offenhäusser, A.; Mayer, D. Analyzing the electroactive surface of gold nanopillars by electrochemical methods for electrode miniaturization. *Electrochim. Acta* **2008**, *53*, 6265-6272.

(20) Park, J. Y.; Sacha, G.; Enachescu, M.; Ogletree, D.; Ribeiro, R.; Canfield, P. C.; Jenks, C. J.; Thiel, P. A.; Sáenz, J.; Salmeron, M. Sensing dipole fields at atomic steps with combined scanning tunneling and force microscopy. *Phys. Rev. Lett.* **2005**, *95*, 136802.

(21) Petri, M.; Kolb, D. M.; Memmert, U.; Meyer, H. Adsorption of mercaptopropionic acid onto Au (1 1 1): Part I. Adlayer formation, structure and electrochemistry. *Electrochim. Acta* **2003**, *49*, 175-182.

(22) Mayer, D.; Ataka, K.; Heberle, J.; Offenhäusser, A. Scanning probe microscopic studies of the oriented attachment and membrane reconstitution of cytochrome c oxidase to a gold electrode. *Langmuir* **2005**, *21*, 8580-8583.

(23) Colson, A. O.; Besler, B.; Sevilla, M. D. Ab initio molecular orbital calculations on DNA base pair radical ions: Effect of base pairing on proton-transfer energies, electron affinities, and ionization potentials. *J. Phys. Chem. B* **1992**, *96*, 9787-9794.

(24) Singh, A.; Snyder, S.; Lee, L.; Johnston, A. P. R.; Caruso, F.; Yingling, Y. G. Effect of Oligonucleotide Length on

the Assembly of DNA Materials: Molecular Dynamics Simulations of Layer-by-Layer DNA Films. *Langmuir* **2010**, *26*, 17339-17347.
(25) Shakil, S.; Khan, R.; Zarrilli, R.; Khan, A. U. Aminoglycosides versus bacteria–a description of the action, resistance mechanism, and nosocomial battleground. *J. Biomed. Sci.* **2008**, *15*, 5-14.
(26) Anne, A.; Bouchardon, A.; Moiroux, J. 3 '-ferrocene-labeled oligonucleotide chains end-tethered to gold electrode surfaces: novel model systems for exploring flexibility of short DNA using cyclic voltammetry. *J. Am. Chem. Soc.* **2003**, *125*, 1112-1113.
(27) Balamurugan, S.; Obubuafo, A.; McCarley, R. L.; Soper, S. A.; Spivak, D. A. Effect of linker structure on surface density of aptamer monolayers and their corresponding protein binding efficiency. *Anal. Chem.* **2008**, *80*, 9630-9634.
(28) Steel, A.; Levicky, R.; Herne, T.; Tarlov, M. J. Immobilization of nucleic acids at solid surfaces: effect of oligonucleotide length on layer assembly. *Biophys. J.* **2000**, *79*, 975-981.
(29) Shi, X.; Wen, J.; Li, Y.; Zheng, Y.; Zhou, J.; Li, X.; Yu, H.-Z. DNA molecular beacon-based plastic biochip: a versatile and sensitive scanometric detection platform. *ACS Appl. Mater. Interfaces* **2014**, *6*, 21788-21797.
(30) Walter, J.-G.; Kökpinar, O. z.; Friehs, K.; Stahl, F.; Scheper, T. Systematic Investigation of Optimal Aptamer Immobilization for Protein– Microarray Applications. *Anal. Chem.* **2008**, *80*, 7372-7378.
(31) Lao, Y. H.; Peck, K.; Chen, L. C. Enhancement of aptamer microarray sensitivity through spacer optimization and avidity effect. *Anal. Chem.* **2009**, *81*, 1747-1754.
(32) Yu, Z.-g.; Sutlief, A. L.; Lai, R. Y. Towards the development of a sensitive and selective electrochemical aptamer-based ampicillin sensor. *Sensor Actuat. B Chem.* **2018**, *258*, 722-729.
(33) Sumner, J. J.; Creager, S. E. Redox Kinetics in Monolayers on Electrodes: Electron Transfer Is Sluggish for Ferrocene Groups Buried within the Monolayer Interior. *J. Phys. Chem. B* **2001**, *105*, 8739-8745.

Table of Contents artwork